

NLTE calculations of neutral helium lines in the wind of the Herbig Ae star AB Aurigae

J.-C. Bouret^{1,2} and C. Catala¹

¹ Laboratoire d'Astrophysique de Toulouse, CNRS UMR 5572, Observatoire Midi-Pyrénées, 14, avenue Edouard Belin, 31400 Toulouse, France

² NASA/Goddard Space Flight Center, Code 685, Greenbelt, MD 20771, USA

Received 17 January 2000 / Accepted 25 May 2000

Abstract. In order to improve our knowledge about the structure of the winds of the Herbig Ae/Be stars and the mechanisms that drive them, we performed a NLTE analysis of the formation of helium lines in the wind of AB Aur, the prototype of the whole class. These lines are indeed expected to form in the densest layers of the envelope, at the very base of the wind, and therefore to provide constraints on these regions where the wind originates. A large observational data set is now available which we have extensively used to deduce strong constraints on the physics that prevail in the inner part of the wind. Among these data, we particularly used those from the MUSICOS 1996 campaign, which show that the He I D3 ($\lambda 5876 \text{ \AA}$) line is made of two distinct components: a blue-shifted emission component, and a redshifted component alternatively seen as an absorption or an emission.

The classical model for AB Aur's wind (Bouret & Catala 1998; Catala & Kunasz 1987) fails to reproduce the observed profile. We find that the observations can be explained by a two component model in which the base of the wind includes dense and hot clumps of outflowing material, while the bulk of the wind is still described by the model by Bouret & Catala (1998). This clumpy structure can result from the presence of co-rotating interaction regions which form where fast streams in the wind overtake slow streams. Our results show that a blue-shifted

emission is formed in such conditions, and can be rotationally modulated as observed, due to fast and slow streams alternating on the line of sight as the star rotates.

Our model can also explain the occasional presence of an absorption component near rest wavelength, as formed in the bulk of the extended chromosphere. Concerning the red emission component, which is occasionally observed instead of the absorption one, we argue that it may arise from polar downflows.

Key words: line: formation – line: profiles – stars: atmospheres – stars: chromospheres – stars: mass-loss – stars: pre-main sequence

1. Introduction

The Herbig Ae/Be (HAeBe) stars are pre-main sequence objects of intermediate mass. One of the observational criteria used to define this class is the presence of a rich emission line spectrum (Herbig 1960; Thé et al. 1994). A significant fraction of the HAeBe present PCygni profiles at H α and MgII h & k resonance lines (Finkenzeller & Mundt 1984; Catala et al. 1986b) which demonstrate that these stars experience phases of mass loss through stellar winds. In addition to these conspicuous wind features, these stars also present signatures of high temperature regions in their envelopes, such as Si IV, C IV lines in absorption, or N V, Ca II infrared triplet and He I D3 lines in emission (Catala et al. 1986a; Hamman & Persson 1992; Bouret et al. 1997). We shall call these characteristics “active phenomena” in the following.

The past two decades have seen important efforts to understand these active phenomena, which could help define the place of HAeBe in the context of stellar evolution towards the main sequence.

A first class of models postulate an external origin for these winds, high ionization and emission phenomena, invoking an accretion disk (Hillenbrand et al. 1992; Marsh et al. 1995; Grinin & Rostopchina 1996; Corcoran & Ray 1998).

An accretion disk may indeed drive a radiative wind with adequate mass loss rates and terminal velocities, as suggested by Proga et al. (1998) and Drew et al. (1998) for intermediate mass protostars.

It has been also shown (Croswell et al. 1987) that PCygni profiles could be produced in disk winds, provided a disk chromosphere is present, which helps to produce the emission component of the PCygni profile.

Moreover, according to a model first proposed for classical T Tauri stars (CTTS), the source of the observed active phenomena could be found through the release of the disk gravitational energy in a boundary layer at the stellar surface (Bertout et al. 1988; Basri & Bertout 1989). Alternatively, magnetospheric accretion (Königl 1991; Shu et al. 1994; Hartmann et al. 1994), could also explain the appearance of emission lines (He I D3, O I $\lambda 7773$ and $\lambda 8846$...) in HAeBe spectra.

However, the presence of accretion disks around HAeBe is still uncertain. The disk model invoked by Hillenbrand et al. (1992) to account for the infrared excesses of the HAeBe has been criticized by Berrilli et al. (1992) and Hartmann et al. (1993), who explain the observed IR excesses with spherical dust envelopes. More recently Pezzuto et al. (1997) showed that the spectral energy distribution of a large group of Herbig Ae/Be stars is well explained by a spherically symmetric model for matter distribution, the dust being constituted by noncrystalline particles. Böhm & Catala (1994) and Corcoran & Ray (1997) observed that those HAeBe that are less deeply embedded in their parental cloud exhibit symmetric and unshifted forbidden [O I] lines, in contrast to the majority of CTTS or the deeply embedded HAeBe, which show strongly asymmetric and blueshifted forbidden lines. Such asymmetries and blueshifts are interpreted as evidence for an optically thick accretion disk that hides the receding half of a wind in which the forbidden lines are formed (Appenzeller et al. 1983, 1984). Finally, longslit observations by Böhm & Hirth (1997) ruled out the possibility for the [O I] lines of some HAeBe to be formed in an extended thin region at the surface of an accretion disk.

On the other hand, elongated structures of several hundred AU have been detected around some HAeBe, using high angular resolution millimeter observations (Mannings & Sargent 1997), which probably indicates the presence of extended circumstellar disks for these objects. Whether these remote disk-like structures can play a role in powering the active phenomena discussed above still remains to be investigated.

We note in this respect that recent near infrared interferometric observations of AB Aur, the prototypical Herbig Ae star, seem to exclude classical accretion disk models for the sub-AU structure of its circumstellar environment, and favor a moderately flattened distribution of matter (Millan-Gabet et al. 1999).

Evaporating falling bodies have been invoked to explain some spectral characteristics of HAeBe, like the red absorption components of the NaD doublet at 5900 Å (Sorelli et al. 1996). They have also been assumed to be responsible for the spectroscopic and photometric variability of these stars (Skrutskie et al. 1996; Grady 1996 et al., 1999). However, they cannot account for most of the active phenomena discussed here, such as, e.g., the CIV and NV resonance doublet, blue-shifted with respect to their rest wavelengths. Finally, the spectral features produced by such infalling bodies are formed at distances higher than 5 stellar radii, which leaves unexplored the regions in the immediate vicinity of the stars, where the outflow and the active phenomena originate from.

Alternately, several authors have suggested that the source of energy responsible for the observed active phenomena lies inside the star, rather than in its circumstellar environment. A model has been proposed by Vigneron et al. (1990), then revisited by Tout & Pringle (1995), and completed recently by Lignières et al. (1996), in which rotational braking of the star via a strong stellar wind excites turbulent motions below the star's surface. These turbulent motions would be responsible for a dynamo that generates the magnetic field needed to sustain activity. In this model, which assumes that the activity is

magnetic, the ultimate source of energy is the star's internal rotation.

Among the HAeBe, AB Aurigae (A0 Ve+sh; Thé et al. 1994) is often considered as the prototype of the HAeBe with P Cygni profiles (the P Cygni subclass). Because of the straightforward interpretation of its strong PCygni profiles as formed in a wind and because of its rather complete observational (spectral and temporal) coverage, AB Aur is suitable for a precise modelling.

In a first attempt to model the wind of this star, Catala et al. (1984), Catala & Kunasz (1987), and Catala (1988), using the Mg II and C IV resonance lines, as well as H α , suggested that it is spherically symmetric, with a mass loss rate of about $10^{-8} M_{\odot} \text{yr}^{-1}$, and includes an extended chromosphere of moderate temperature ($T=17,000$ K). Since then, this model has been successfully extended to three other HAeBe of the PCygni subclass (Bouret & Catala 1998); radiative losses of a few percent of the total stellar luminosity were found, which are of the same order of magnitude as what is found in CTTS (Calvet & Albarran 1984; Bouvier 1987).

There is growing evidence that magnetic fields play an important role in controlling the active phenomena of HAeBe. First of all, rotational modulation of lines formed in the wind of several HAeBe, including AB Aur, was reported (Praderie et al. 1986; Catala et al. 1986b, 1989, 1991; Beskrovnyaya et al. 1995; Böhm et al. 1996). This modulation is interpreted in terms of corotating streams controlled by a surface magnetic field. Second, Donati et al. (1997) have recently reported the direct detection of a surface magnetic field in the southern Herbig Ae star HD 104237.

It has been suggested that the corotating streams responsible for the rotational modulation in AB Aur, also give rise to corotating interaction regions (CIRs), similar to those of the solar wind (Catala et al. 1986b). Such CIRs have been shown to be able to explain the N V and X-ray emission, respectively observed with HST/GHRS and ROSAT, which cannot be produced by the model of Catala & Kunasz (Zinnecker & Preibisch 1994; Bouret et al. 1997). An appealing alternative to this interpretation is a magnetically confined wind, such as the one suggested by Babel & Montmerle (1997) for the Ap star IQ Aur. In the framework of this model, the N V resonance lines and the X-ray flux would be formed in a post-shock region in the magnetic equatorial plane, where magnetically channelled streams from the two hemispheres collide.

The influence of a magnetic field on the structure of the wind has also been invoked to explain the behaviour of the H α line of AB Aur, which has been shown to vary from a typical type II PCygni profile to a single-peak emission profile (Beskrovnyaya et al. 1991, 1995). The equatorial wind model proposed by Pogodin (1992) assumes that the wind is confined to equatorial regions by a magnetic field whose opening angle is variable. Each time the line of sight intercepts the wind region, a PCygni profile is formed, while a single-peak emission profile appears otherwise.

More recently Strafella et al. (1998) investigated the combined effects of several acceleration mechanisms, like thermal expansion, radiative pressure, centrifugal acceleration by a coro-

tating magnetic field and hydromagnetic waves, on the emergence of the winds of HAeBe. Calculating line profiles for H α in AB Aur's case, they were able to qualitatively reproduce the aforementioned variations and suggested a value of $B \approx 30\text{--}40\text{G}$ for the strength of the magnetic field (at the star's poles).

Clearly, a better understanding of the mechanisms at work in AB Aur and the other HAeBe requires a better and more reliable description of the physical conditions prevailing in their winds (densities, velocity fields, temperatures, magnetic fields). Some of this can be achieved by modelling quantitatively spectral lines formed in these winds. Although observational evidence is accumulating that the structure of these winds is complex and involves 3D structures, simpler 1D and 2D models are still necessary to understand the physical conditions in which the spectral lines are formed. Moreover, we can take advantage of the fact that various spectral lines probe various density and temperature regimes to study separately the different components of the winds of these stars. All the constraints obtained separately on these different components can be then assembled to build a complete model.

The goal of the present work is to provide a first analysis of the formation of He I lines in the winds of HAeBe, represented by the prototypical AB Aur. These lines are one of the fundamental pieces of the puzzle, not only because of their mere presence around an A0Ve star like AB Aur (the UV radiation field from such stars is indeed too weak to populate significantly the excited levels of He I, so that collisional processes are needed to produce He I lines), but also because of their very peculiar variability which allows us to probe in detail characteristic phenomena occurring at the base of the wind.

In Sect. 2, we review the results of previous related work and summarize the main properties of the He I D3 line in AB Aur's wind. Sect. 3 is devoted to a description of the modelling tools we have used and to the influence of the atomic model on the line profile. The whole set of results we obtained is presented in Sect. 4, together with comments on the physics of the He I line formation. A general conclusion, as well as some implications of the present calculations on our understanding of the physical properties of the wind, are given in Sect. 5.

2. The He I lines in AB Aur

The presence of the He I 5876 Å line in AB Aur has been known for a long time (see e.g. Felenbok et al. 1983; Catala et al. 1984). The line exhibits a complex structure, that can be subdivided in two components. The first component is a blueshifted broad emission (up to 300 km s^{-1} Catala et al. 1993), which is always observed. The second one is a slightly redshifted component, either in absorption or in emission. Although the absorption component is of non photospheric origin, its width seems consistent with a broadening due to stellar rotation alone; this behaviour is also observed in a large sample of HAeBe (Böhm & Catala 1995). This leads us to the first conclusion that the region where this component is formed is very close to the photosphere.

More recently, the observations from the 1996 MUSICOS campaign (Catala et al. 1999) have shown (i) that the blue emis-

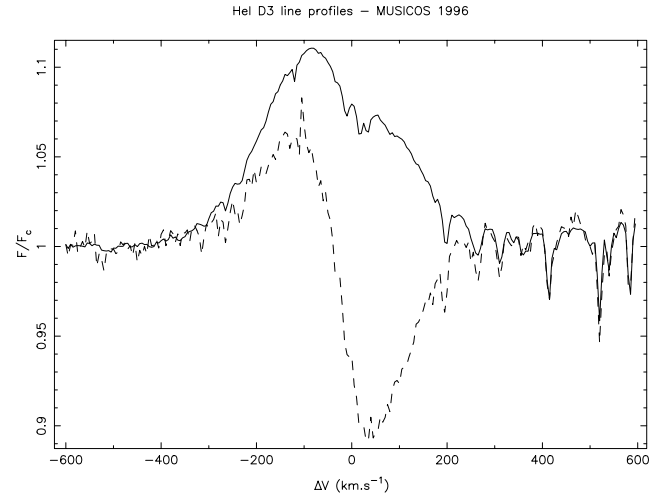


Fig. 1. Observed profile of the He I D3 line, during the MUSICOS 96 campaign. The profile shown in full line is an average of all the spectra obtained during the campaign. One particular spectrum obtained during this campaign, and showing an absorption component centered near zero velocity, is shown in dashed line.

sion of the He I D3 line is modulated in velocity with a 45hr period; (ii) that the red component, alternating from emission to absorption, does not vary significantly in velocity but rather in intensity, with a possible 45hr periodicity. In addition, the variations of the equivalent width of this component are well correlated with those of the photospheric lines.

Fig. 1 presents the He I D3 lines of AB Aur, as observed during the MUSICOS 96 campaign. The profile displayed in solid line in this figure is an average of all the spectra obtained during several days, and therefore is representative of the average structure of its line formation region. The profile shown in dashed line corresponds to one particular spectrum obtained during the campaign, and shows the high level of variability of this He I line during the campaign.

Two interpretations were proposed by Catala et al. (1999) for the behaviour of the blue component. In the first one, this component is formed at the base of a wind originating from the equatorial regions of the star, with a variable aperture angle (see Pogodin 1992). The observed modulation is then caused by the presence of stream structures, analogous to those already invoked to explain the modulation seen in the Mg II resonance lines (Praderie et al. 1986), and the presence of N V lines and X-ray emission through CIR (Bouret et al. 1997).

The other interpretation requires the presence of a rotating circumstellar disk, from which the stellar wind is originating (see Proga et al. 1998; Drew et al. 1998). In this model, the period of modulation of the He I D3 line is that of the disk rotation in the regions from where the wind originates. Using the observed modulation period and the modulation amplitude (200 km s^{-1}) as well as an inclination angle of about 70° (Mannings & Sargent 1997), it is possible to infer that the blue component of the He I D3 lines forms in regions of the wind originating from the disks at about $1.6 R_*$ (Catala et al. 1999). This distance may correspond to the inner boundary of the accretion disk.

In addition, Catala et al. (1999) suggest the presence of downflows onto the stellar pole to explain the formation of the red component when seen in emission.

As shown by Hartmann et al. (1994) or Muzerolle et al. (1998), magnetospheric accretion model could also explain the appearance of the He I D3 line with the observed two component profile. Nevertheless, it does not seem possible, in this framework, to explain the observed centroid variations of the blue component, which always stays blue-shifted. This model, which did not include rotation, show that, as the inclination angle of the disk increases, the emission component gets more and more centered on the rest wavelength, while the absorption becomes more prominent. If rotation was to be included, it is very likely that the emission component would be modulated in velocity, alternating from blue to red as the star rotates, which is not observed. This strengthens the interpretation that the blue component and the red one result from different mechanisms.

All these models are qualitative, and the question of whether the He I D3 lines can indeed be formed in these models with their observed characteristics is still awaiting quantitative confirmation. In this paper, we focus mainly on the equatorial wind model. Indeed, there are so far no decisive arguments against a (more or less) spherical wind, to explain the observed phenomena in AB Aur. It is therefore legitimate to test, improve and refine the existing model of AB Aur's wind, by modelling new lines and atomic species. We performed radiative transfer calculations to check the capability of this model to indeed produce both a blue-shifted emission component behaving like the observed one and an absorption component redward of the rest wavelength. We also checked that episodic accretion onto the stellar pole can produce the observed redshifted emission component. The quantitative modelling of the disk-wind model is beyond the scope of this paper, and will be treated later.

Other He I lines of the optical spectrum can be used in this analysis. The λ 4471 Å line (triplet) is seen in absorption and deeper than the Kurucz model corresponding to AB Aur (Böhm & Catala 1993). The singlet λ 6678 line has the same shape as λ 5876 but with a smaller intensity, while the λ 4921 is not observed at all, probably because it is blended with the strong Fe II lines in this spectral range (Böhm & Catala 1993). Finally, we note that the He II 1640 Å line is absent from the IUE archive spectra.

In summary, a model of the formation of the He I-He II lines in the wind of AB Aur must comply with the following constraints:

1. The He I D3 line always has a blue-shifted emission component with an average velocity of approximately -100 km s^{-1} and an average intensity above the continuum level of $F/F_c = 1.1$. This velocity of the blue-shifted component is modulated with a period near 45 hrs (Catala et al. 1999).
2. The He I D3 line also often exhibits a red-shifted emission component with a velocity near $+100 \text{ km s}^{-1}$, modulated in intensity but not in velocity (Catala et al. 1999).
3. This red-shifted emission component sometimes disappears, revealing a slightly redshifted absorption component, with a width compatible with the measured projected rotation velocity of the star.
4. The He II λ 1640 Å line does not appear on the IUE archive spectra of AB Aur, indicating that its intensity must be $F/F_c \leq 1.1$. This line must therefore be less intense than the He I D3 line.
5. The He I 4471 Å appears in absorption, slightly deeper than the one given by Kurucz models for AB Aur's parameters (Böhm & Catala 1993).
6. The other lines and continua of AB Aur (hydrogen Balmer lines, hydrogen continua, Mg II and C IV resonance lines), used in previous analysis (Catala & Kunasz 1987; Catala 1988; Bouret & Catala 1998) and reasonably well reproduced by the "standard" Bouret & Catala (1998) (hereafter BC) model, must not be affected by any additional features to this model.

3. Modelling the He I - He II spectrum

3.1. Wind model and radiative transfer

In a first step, it is necessary to build a set of models for the wind of AB Aur, that will provide the physical quantities needed to perform radiative transfer calculations. The models we used are constructed in the same way as in BC. The reader is referred to this paper for more details. These spherically symmetric models include an extended chromosphere, located above the minimum of temperature of the photosphere, and surrounded by an isothermal cooler region. The chromospheric radius R_{ch} is the one where the maximum of temperature T_{max} is reached. The velocity law is monotonically increasing outward. Additionally, we used another parameter, the Doppler random velocity v_D , to describe turbulent motions in the wind. This parameter acts as a non thermal broadening component. The photosphere at the base of the wind is simulated by a Kurucz model (1979) with $T_{eff} = 10,000 \text{ K}$ and $\log g = 4.0$.

After the model is constructed, it is possible to calculate the line profiles, taking into account NLTE effects. We carried out this step with the ETLA code, which solves the radiative transfer equation in the comoving frame of the wind, in the equivalent two level atom formulation (Mihalas & Kunasz 1978). The output from ETLA (populations of atomic levels, source functions and opacity in lines and continua...) are used to calculate emergent intensities of interest, in the observer's frame. The corresponding emergent fluxes are then obtained by integrating the emergent intensities on a set of rays parallel to the line of sight from the observer (see Catala & Kunasz 1987 for details).

3.2. The atomic model

We also had to build an atomic model, that is to say we had to choose among the atomic levels, those which are relevant to the calculations we intend to perform. He I was then represented by 29 levels; all the LS states up to $n = 5$ were introduced and

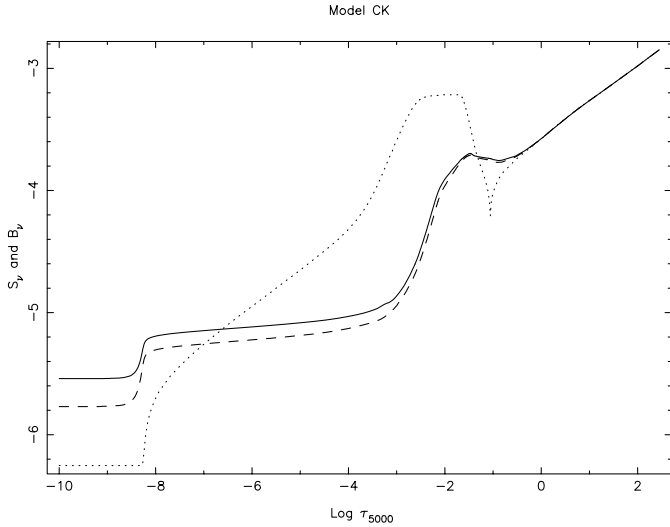


Fig. 2. Computed source function of the He I D3 line with 29 levels (full line) and with 19 levels (dashed line). The Planck function (dotted line) for the model BC is shown to indicate the temperature law.

treated as separate levels. He II was assumed to be a 5 level atom. Finally, we also introduced the single state of He III.

It is worth mentioning that the atomic data that are currently available are reliable for the levels up to $n = 4$ only. Above $n = 4$, the intrinsic accuracy of these data considerably decreases (Berrington & Kingston 1987) and little is known about the influence of the highly excited levels on the spectrum of helium.

Oscillator strengths and energy levels for both He I and He II are from Wiese et al. (1966). For bound-bound transitions of He I, we used collision cross-sections from Berrington & Kingston (1987), up to $n = 4$. The inclusion of the $n = 5$ and $n = 6$ levels was achieved thanks to a program written by Sahal-Br echot (private communication) and based on the Seaton approximation (1962). For a few transitions involving levels with $n = 5$, we also used data from Benson & Kulander (1972). Concerning the collisional ionization rates from levels of He I, we used the data and relations from Mihalas & Stone (1968). The collisional rates (bound-bound and bound-free) of He II were taken from TLUSTY code (Hubeny 1988). The source of the photoionization cross-sections of He I is the Opacity project database (Fernley et al. 1987), while for He II (hydrogenic ion, $Z = 2$), we took the same form as for hydrogen (cf. Mihalas 1978).

We assumed a Voigt profile for the line; the natural damping parameter was written following the classical expression: $a = 2.47342 \times 10^{-22} \nu^2 / 4\pi \Delta\nu_D$, where ν is the frequency of the line and $\Delta\nu_D$ is the Doppler broadening.

Although the atomic data for levels with $n = 5$ and $n = 6$ are approximate, the inclusion of these levels provides a better description of the transitions involving levels with $n = 4$ and $n = 5$ respectively and for the recombination cascades as well. The influence of these levels on the line formation will now be discussed, for the best fit model of AB Aur’s wind obtained by BC, which we will consider as the reference model in the following. We present in Fig. 2 the run with the optical depth of

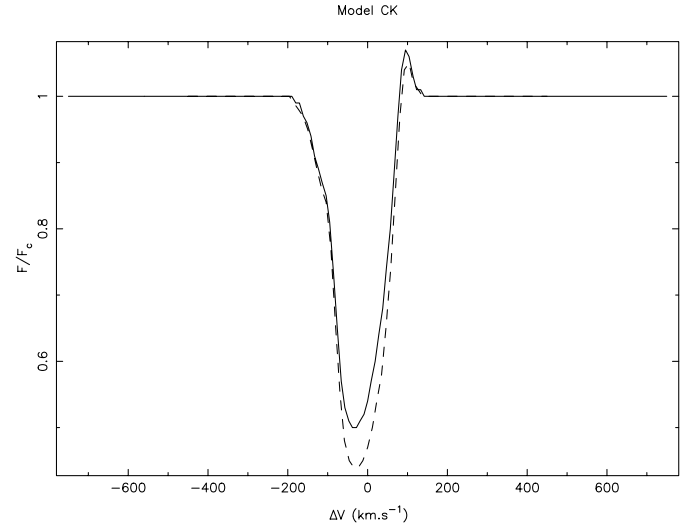


Fig. 3. Computed profiles of the He I D3 line for the model BC; 29 levels (full line) and 19 (dashed line)

the line source function, for a model with 19 levels (up to $n = 4$), compared to that obtained with the model used for this work. In the bulk of the chromosphere, S_ν with our 29 levels atomic model is notably higher than what is produced when only 19 levels are considered. The consequences on the line profile are shown in Fig. 3. Clearly, the inclusion of high lying levels plays an important role in the line strength. In the present case, the change is of 12 the emission component. We have checked that this effect exists for even higher temperatures, by performing the same kind of calculations for a model with $T_{max} = 40,000$ K.

Considering this important impact on the resulting source function and the line profile, we used an atomic model with 29 levels for He I in all the calculations described in this paper.

4. Results

4.1. The standard BC model

The “standard” BC model was built to reproduce lines and continua formed in the wind of AB Aur and in the bulk of its chromosphere (hydrogen Balmer lines, hydrogen continua, Mg II and C IV resonance lines). These results confirmed those obtained by Catala & Kunasz (1987) as well as mass loss rate estimates based on radio continuum observations (Skinner et al. 1993), and the parameters derived for the wind and the chromosphere of AB Aur seem therefore quite reliable.

As can be seen from Fig. 3, the standard BC model for AB Aur does not produce any blue emission component in the He I D3 line, but rather a P Cygni type profile, with a blueshifted absorption component and a weak redshifted emission component. Such a model is therefore inadequate to explain the characteristics of the observed He I D3 lines in AB Aur. A close examination of the results obtained with this model indicates that the source function does not rise sufficiently in the chromospheric region to yield a blue emission component (see Fig. 2). Therefore, on the rays that hit the stellar core (see Sect. 3.1), the

specific intensity in the line is always lower than in the adjacent continuum, contributing in the emergent flux to the strong blueshifted absorption component seen on Fig. 3. It is clear from Fig. 2 that NLTE effects in the temperature maximum region tend to decrease strongly the line source function, resulting in the strong absorption component seen in Fig. 3. The standard BC model is based on a quantitative interpretation of lines formed in the wind and the maximum temperature region of the chromosphere, and the regions near the base of the chromosphere and the temperature minimum are not well constrained in this model. It is therefore very natural to investigate what physical conditions in these loosely constrained regions could give rise to the observed characteristics of the He I D3 line.

4.2. Departures from the standard BC model

4.2.1. Results with a hot ($T \approx 140,000$ K) region

Recent observations with the HST/GHRS have shown the presence of N V resonance lines in AB Aur, indicating the presence of high temperature regions in its wind (Bouret et al. 1997). The N V lines were used to constrain these hot regions, and it was proposed that they result from shocks produced in co-rotating interaction regions (CIR) in the wind of AB Aur. These CIR may also be responsible for the observed X-ray emission of AB Aur, detected by ROSAT (Zinnecker & Preibisch 1994). The hot regions created by the CIR are not spherically homogeneous, but rather encompass only a small fraction of the wind volume, resulting in small filling factors for the N V line emitting region. By analogy with the solar case, it is generally assumed that CIRs are generated by the presence in the wind of shocks between fast and slow streams of material, the latter being confined by the surface magnetic field of the star (Mullan 1984). Unlike the solar case, the CIRs of AB Aur can be located very close to the star's surface (Catala et al. 1986b). The rotational modulation of the He I D3 line (Böhm et al. 1996; Catala et al. 1999) and of other lines formed in the wind (Praderie et al. 1986; Catala et al. 1986b) is often associated with the presence of such azimuthal structures in the wind of AB Aur, rotating with the star.

In this section, we investigate whether the same type of shock-bounded hot regions can be responsible for the observed He I D3 line characteristics, while being consistent with all other observations available, including the absence of He II lines. We used the model proposed by Bouret et al. (1997), which simulates the CIRs as clumpy hot regions with $T \approx 140,000$ K, and which is able to reproduce the observed N V resonance lines. We find that such models, including a spherically symmetric wind, a moderate temperature (17,000 K) extended chromosphere (similar as the BC model), and a hot (140,000 K) thin clumpy region near the base of the wind, produce an intense He II $\lambda 1640$ Å line, much stronger than the resulting He I D3 line. This is due to the fact that neutral helium is severely depleted in these hot regions, where the helium ionization equilibrium is shifted toward He III. The filling factor for these hot regions derived in Bouret et al. (1997) analysis (7×10^{-3}) is small enough that the resulting He II $\lambda 1640$ Å line falls well below the IUE detection

Table 1. Parameters of models mentioned in the text. Models m1–7 are plotted while models M1–4 are only discussed. R_{hot} , the distance to star center of the maximum temperature (T_{max}) region, is expressed in units of photospheric radius ($R_{ph} = 1.75 \times 10^{11}$ cm), T_{max} is in Kelvin, while the wind velocity reached at that point, $V(R_{hot})$, and the Doppler random velocity v_D are in km s^{-1} . Please refer to BC for details.

Models	R_{hot}	T_{max}	$V(R_{hot})$	v_D	\dot{M} (M_{\odot}/yr)
m1	1.04	25,000	4.	45	1.2×10^{-8}
m2	1.04	33,000	4.	45	1.2×10^{-8}
m3	1.04	40,000	4.	45	1.2×10^{-8}
m4	1.005	20,000	9.	75	3.3×10^{-8}
m5	1.005	24,000	9.	75	3.3×10^{-8}
m6	1.005	30,000	9.	75	3.3×10^{-8}
m7	1.005	30,000	139	10/75	9.6×10^{-6}
M1	1.04	50,000	4.	45	1.2×10^{-8}
M2	1.04	55,000	4.	45	1.2×10^{-8}
M3	1.0025	20,000	100.	75	1.0×10^{-7}
M4	1.015	30,000	100.	75	1.0×10^{-7}

limit of $F/F_C = 1.1$. At the same time, the hot regions do not contribute significantly to the formation of the He I D3 line, which is mainly formed in the cooler parts of the BC chromosphere, and thus ends up with a P Cygni profile similar to that presented in Fig. 3. Conversely, if we assume a higher filling factor for the hot regions, in such a way that the He I D3 emission component reaches the observed intensity, a very intense He II $\lambda 1640$ Å line is formed, in contradiction with its absence in the archive IUE spectra. We therefore conclude that the 140,000 K gas present in the CIR, invoked to explain the observed N V lines, cannot account for the observed He I-He II lines.

4.2.2. Formation of a blue emission component in the He I D3 line

We need to investigate in detail what physical conditions are required to produce a blue emission component in the He I D3 profile. Clearly, such a component can be obtained only if the line source function near the base of the wind is sufficiently high, as discussed in Sect. 4.1. In order to identify the physical conditions necessary for this rise in the source function, we built models of spherically symmetric winds including hot regions near the base of the wind, and explored systematically the parameter space of these models. The parameters of some of the models used in this analysis, and more particularly discussed in the text, are listed in Table 1.

We find that models in which the hot region is located at the same place as the chromosphere in BC, with temperatures higher than that of the BC chromosphere (models m1–3), still produce PCygni profiles, but also include a blue bump increasing in intensity until $T_{max} \approx 50,000$ K (model M1), then decreasing as we checked with the results obtained with model M2. As soon as $T_{max} \approx 40,000$ K (Fig. 4), this blue bump is strong enough to be in emission, yielding a P Cygni type III profile, in the Beals (1950) classification, but with an additional

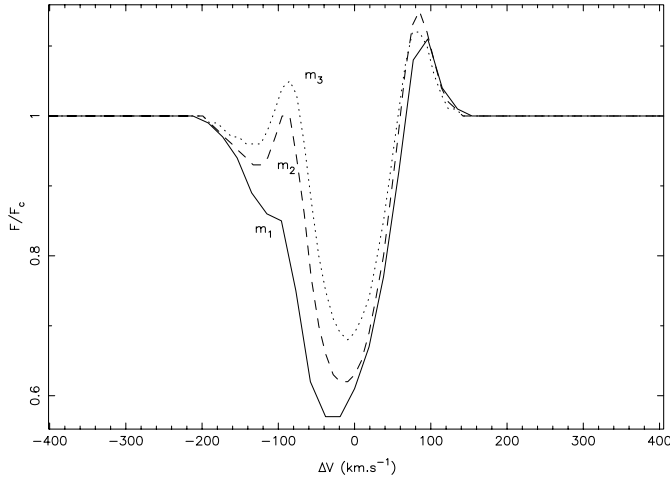


Fig. 4. Three profiles for models with $T_{max} = 25,000$ K (m1, full line), $T_{max} = 33,000$ K (m2, dashed line) and $T_{max} = 40,000$ K (m3, dotted line). The blue bump clearly develops as T_{max} increases.

blueward absorption. These models fail to produce as intense a blueshifted emission component as observed, basically because the line source function is always too low in the regions forming the He I D3 line, and therefore they do not provide the required physical conditions to account for the observed characteristics of this line.

Models with hot regions closer to the star than the BC chromosphere, with small velocity gradients within the hot region (m4–6), yield double peak emission profiles for the He I D3 line, which appear as a wide and symmetrical emission with a central absorption component. Fig. 5 displays profiles produced by different temperature maximum (reached at the same distance from the photosphere). Increasing T_{max} mainly changes the level of the central depression with respect to the continuum level. This effect is easy to understand if one considers the emergent specific intensity on the rays that hit the stellar disk. For model m4, the specific intensity profile on the central ray is still mainly in absorption, again because the line source function in the line forming region is too low. The specific intensity profile turns in emission at higher values of the impact parameter, but is far from being intense enough to fill in the absorption produced on the central rays, and the resulting flux profile appears as a double peak emission, whose central depression reaches below the continuum level. For models m5 and m6, in which the temperature maximum is higher, the line source function increases, and the specific intensity profile on central rays is a double peak emission with a central depression above the continuum level. The resulting flux profile is therefore still a double peak emission, but with a central depression reaching above the continuum level. These models produce a blue emission component with a high intensity, and for models with $T_{max} \leq 30,000$ K no significant He II $\lambda 1640$ Å line is produced, as required. However, the He I D3 line is entirely formed in low wind velocity regions ($V \leq 40$ km s $^{-1}$), the presence of the blue and red emission component being simply due to the large turbulent velocities assumed in these models. It is therefore impossible to explain

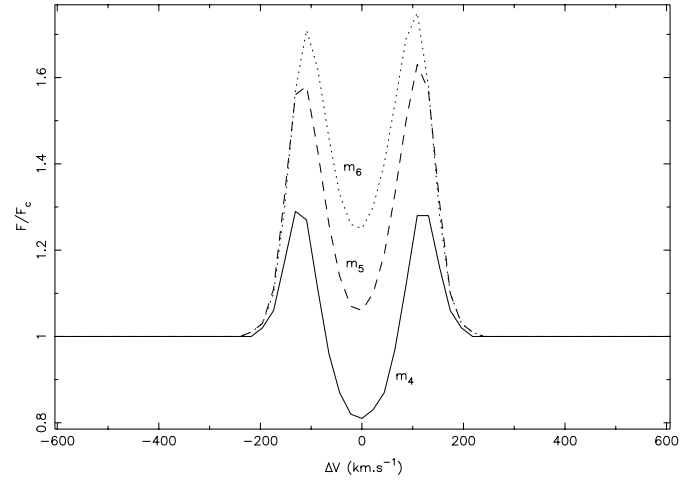


Fig. 5. Profiles for three models with increasing temperatures ($T_{max} = 20,000$ K (m4), $24,000$ K (m5) and $30,000$ K (m6) respectively) reached closer to the star's surface than for models of Fig. 4. The influence of T_{max} on the central depression appears clearly.

Table 2. Velocity laws in km s $^{-1}$

r/R_{ph}	BC 1998	BC99	m7
1	0.001	0.001	0.001
1.005	-	-	139
1.020	-	-	168
1.057	-	-	170
1.01	0.7	7	-
1.1	8	8	180
1.2	50	50	190
1.3	100	100	-
1.5	114	114	-
2.5	150	150	200
50	290	290	290
70	300	300	300

the presence of the observed velocity rotational modulation for the blue emission component in the framework of these models.

We have also checked the effect of increasing the extension of the hot region. For the models producing double peak profiles, extending the hot region only contributes to produce an additional absorption trough, blueward of the blue emission component.

Clearly, the only way to obtain a blue emission component formed in high velocity wind regions, so that it can possibly be modulated in velocity during the star's rotation by the alternation of fast and slow streams, is to increase the velocity gradient of the model in the hot region at the base of the wind, while keeping the density to high values in this region. In our models, the presence of such rapid and dense regions can be simulated by artificially increasing the mass loss rate above the standard value of the BC model. For models with gas velocities higher or equal to 100 km s $^{-1}$ at the point where T_{max} is reached (models M3–4, m7, see Table 2 for the adopted velocity law in this latter case), it is possible to obtain a blue-shifted emission for the He I D3 line. The requirement is that the density of the region

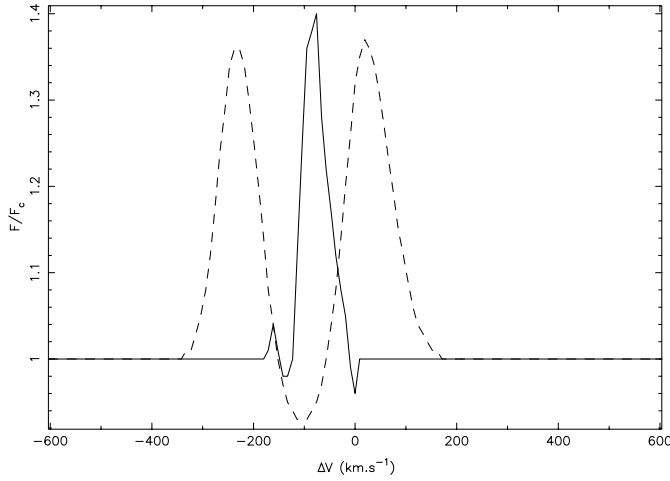


Fig. 6. Profiles for models (m7) only differing by the value of v_D . In one case ($v_D = 10 \text{ km s}^{-1}$, full line), the line is clearly dominated by a blue-shifted emission, while in the other case ($v_D = 75 \text{ km s}^{-1}$, dashed line) we rather obtain a double peak emission profile, although with a significant blue-shift.

of maximum temperature is higher than $1.63 \cdot 10^{-12} \text{ g.cm}^{-3}$, which can be simulated in our model by artificially imposing a mass loss rate higher than $10^{-7} M_{\odot} \cdot \text{yr}^{-1}$. In these models, the Doppler random velocity plays a fundamental role in the appearance of the line either as a classical double peak emission with a blueshifted central depression, or as a profile dominated by a blueshifted emission, as shown in Fig. 6.

Understanding the formation of such profiles requires a close examination of both the line source function and of the specific intensity profiles of different rays (Figs. 7 and 8 respectively).

Let us first examine the case when the Doppler random velocity is small (full line in Fig. 6). The line source function S_L directly maps on the specific intensity profile, on the central rays (impact parameter $p=0$). Indeed, on the red side of the line, the point where $\tau_{\nu} = 1$ is reached only inside the star; therefore, up to $\Delta V = 0$, there is no contribution to the line. Just above the photosphere, we find regions where the velocity is small and S_L decreases. A small absorption is therefore produced. Proceeding outward, S_L now presents a kind of plateau, while the velocity increases up to about 100 km s^{-1} . This plateau is also seen in the specific intensity profile. Between $v=100 \text{ km s}^{-1}$ and $v=150 \text{ km s}^{-1}$, S_L increases strongly, which contributes to produce a strong blueshifted emission. Further in the wind, in regions corresponding to the external border of the hot region, S_L steeply falls off, which is denoted by the absorption component appearing blueward of the emission component. This type of specific intensity profile is obtained up to the rays that are tangent to the stellar core ($p = p_c \approx R_*$). As p increases, the specific intensity profile changes from a PCygni to a single absorption profile, becoming progressively shallower, until regions where the density of He I is too low to contribute to the line. Central rays have larger weights in the integration of the emergent flux, which explains the final line flux profile.

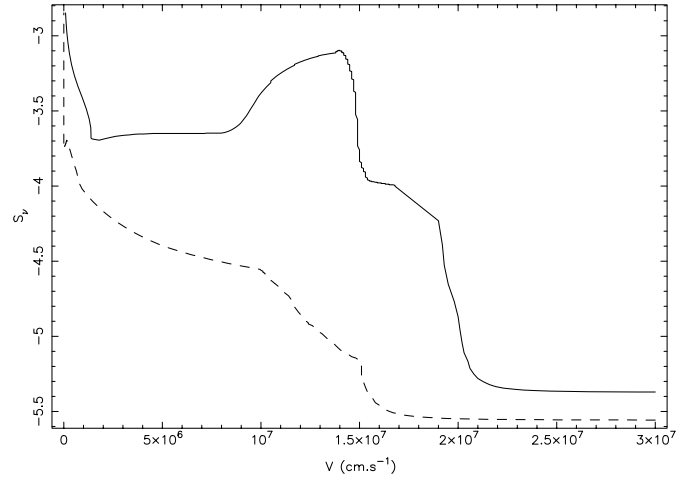


Fig. 7. Run with velocity of the line source function for the model m7 (full line) detailed in the text, producing the profile in full line of Fig. 6. The dashed line is the source function of BC's model.

Models with high values of the Doppler random velocity v_D essentially behave in the same way, except that now both the emission and absorption components produced in the intensity specific profile on the central rays are much wider. In the resulting flux emergent profile, the line thus appears as a wide, intense, and blueshifted emission, in which a wide and blueshifted absorption component is dug (dashed line in Fig. 6). The crucial aspect of these models with high velocity gradients near the base of the wind is the source function rise in a region of high velocity (see Fig. 7), which produces a blueshifted emission component, as observed. In these models indeed, NLTE effects depopulate the lower level ($2p^3P^0$) more efficiently than the upper level ($3d^3D$) in the hot region at the base of the wind. This relative under-population of the lower level is mainly caused by the fact that in this region, the $\lambda 10830 \text{ \AA}$ line is optically thin, which means that many photons in this transition cross the hot region without interacting with atoms. In order to illustrate this effect, we present in Fig. 9 the run with optical depth at 5000 \AA of the departure coefficients for the two levels of the $\lambda 5876 \text{ \AA}$ line. The ratio of the departure coefficients, b_l/b_u , is indeed lower than unity in the hot region near the base of the wind.

Only these models with a deep hot region, and presenting a strong velocity gradient at the base of the wind, as well as high densities in these regions, are capable of producing a strong blueshifted emission component formed in a high velocity wind region, so that we can expect it to be modulated by the star's rotation if fast and slow streams alternate on the line of sight.

4.2.3. Constraints from the He I 4471 \AA line

The profile of the He I 4471 line observed during the MUSICOS 1996 campaign is slightly deeper than the one expected for a Kurucz models with AB Aur's parameter and $v \sin i = 80 \pm 5 \text{ km s}^{-1}$, which is consistent with the observation of Böhm & Catala (1993). This small difference, which is very likely due to a wind contribution to the line, is extremely helpful to derive new

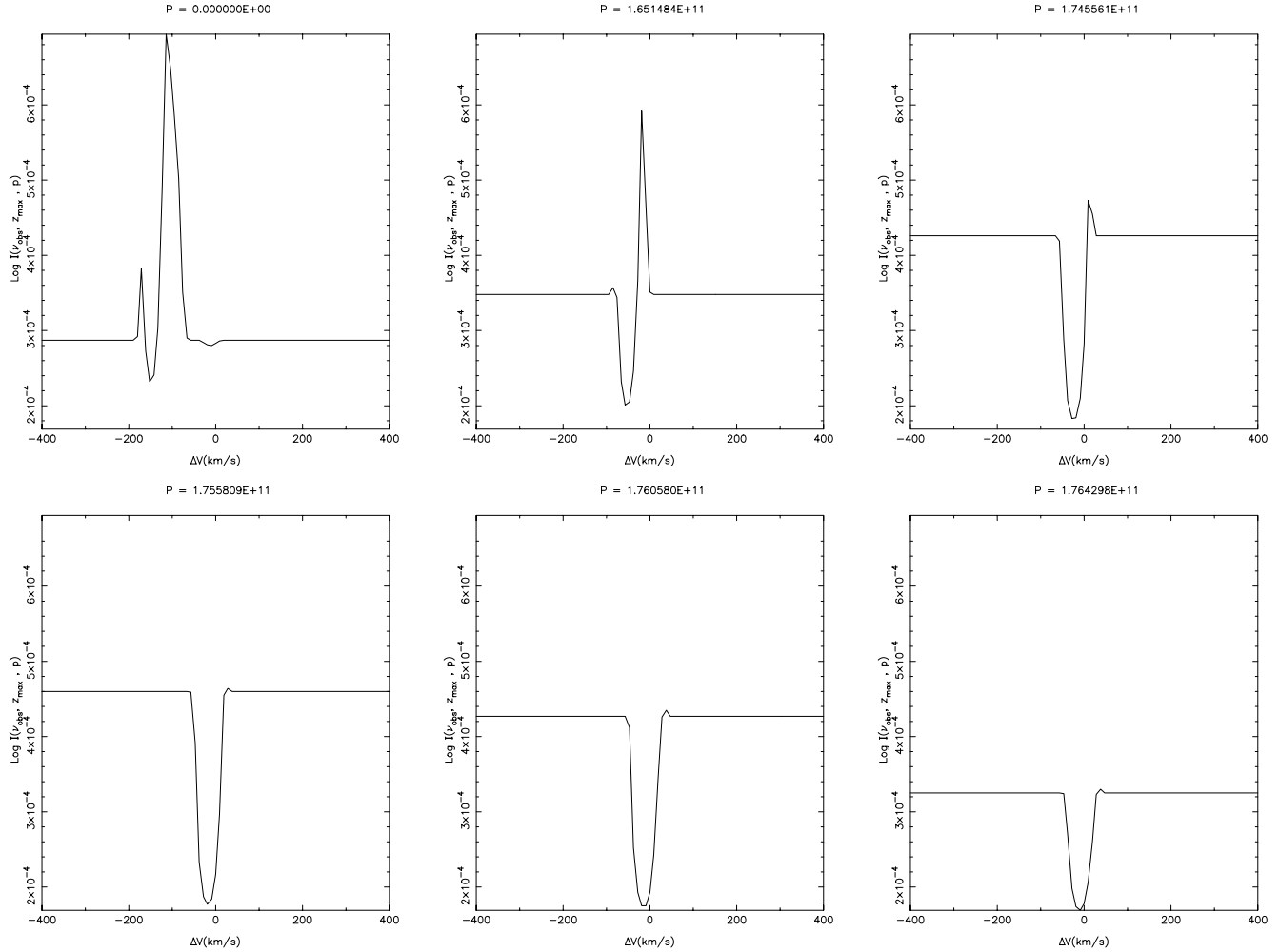


Fig. 8. Evolution of the specific intensity with the impact parameter p (for model m7).

constraints on the density and velocity field at the very base of the wind. Classical models (Catala & Kunasz 1987, BC) produce a line which is much deeper and narrower than the observed one. On the other hand, increasing the velocity gradient in the line formation region (which extends from $0.001R_{ph}$ to $0.003R_{ph}$ above the photosphere) by a factor 2.5 (everything else being kept fixed) in BC, yields a line only slightly deeper than the observed one and wider than in BC model. This change in ∇V in this region is small enough that it does not affect the other lines previously modelled, which are formed in the bulk of the chromosphere. Hence, an important result of this study is that the velocity law in BC model needs to be changed for the model to be consistent with the helium spectrum. More precisely, referring to the table from Catala & Kunasz (1987) for the velocity law (also used in BC), we have to adopt instead the one presented in Table 2. We will refer to this modified BC model as BC99.

In addition, at such a distance above the photosphere, the wind is probably still in corotation with the star and it is therefore very tempting to interpret the difference in depth of the computed and observed He I 4471 line in terms of a rotational broadening (and therefore shallowing) of the line. The line formation region being rather narrow, the final line profile can be

reasonably approximated by a convolution of the profile computed without rotation with a rotation profile with $v \sin i = 80 \pm 5 \text{ km s}^{-1}$ and $\epsilon = 0.6$ (ϵ being the limb-darkening coefficient, see Gray 1992). We found that it is then consistent with the profile observed during the MUSICOS 1996 campaign (Fig. 10).

We also investigated the contribution to this line of the previously described hot-dense regions at the base of the wind. It turns out from our calculations that as long as $\rho \leq 6.1 \times 10^{-10} \text{ g.cm}^{-3}$, the line appears as an absorption line, shifted to the blue with respect to its rest wavelength, which, as we shall see later, would not be inconsistent with the observations. On the other hand, for a value of the density higher than this limit, He 4471 Å appears as a weak emission line shifted toward the blue, which would give to the line the same shape as the one of He I 5876 Å line (see hereafter), that is clearly not observed. We therefore adopted this value as an upper limit on ρ .

4.3. A two-component model

So far, we have established that the base of the wind of AB Aur must be represented by a modified BC model (identified as BC99), in order to remain consistent with the observed He I 4471

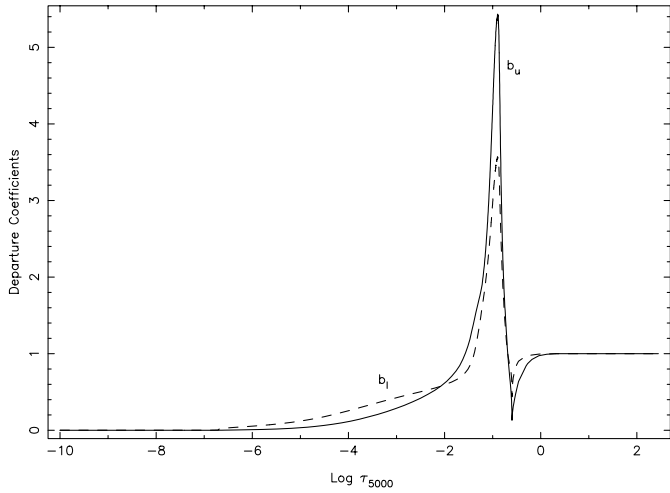


Fig. 9. Departure coefficients for the lower level (dashed line) and upper level (full line) for the $2p\ ^3P^0-3d\ ^3D$ transition, produced by model m7. The ratio b_l/b_u is clearly greater than unity in the hot region at the base of the wind.

line. We have also seen that the observed characteristics of the He I 5876 line, as well as the absence of the He II 1640 line, necessitate an additional deep hot and clumpy region near the base of the wind. More precisely, this additional hot region must be located closer than $1.015R_{ph}$ from the star's center (model M4), otherwise no blueshifted emission can be produced in the He I D3 line, regardless of the temperature. At the same time, the hot region cannot be closer than $1.0025R_{ph}$ from the star's center (model M3), without affecting seriously the formation of all the photospheric features which are well reproduced by a standard Kurucz model (Böhm & Catala 1993). These two values for the location of the hot region can therefore be considered as upper and lower limits, respectively. With the hot region location set at its lower limit, we find that T_{max} must be at least 20,000 K to produce an emission He I D3 line. On the other hand, when the hot region is located at $1.015R_{ph}$, the He II 1640 Å line appears in emission, which is not observed, for values of T_{max} above 30,000 K, which must therefore be considered as the upper limit for T_{max} .

These results, together with those already presented in Sect. 4.2 can be summarized by the following constraints on the model parameters:

- temperature: $20,000\text{ K} \leq T_{max} \leq 30,000\text{ K}$
- location: $1.0025R_{ph} \leq R_{hot} \leq 1.015R_{ph}$
- velocity: $V \geq 100\text{ km.s}^{-1}$
- density: $1.63 \times 10^{-12} \leq \rho \leq 6.1 \times 10^{-10}\text{ g.cm}^{-3}$

The velocity laws assumed in these various models (BC99 for the bulk of the wind; m7 for the hot dense clumps) are given in Table 2.

With these results at hand, we examine below how a two-component model involving a “standard” BC-type wind and chromosphere on one hand, and a set of dense and hot regions with the characteristics detailed above, created by CIR near the base of the wind on the other hand, can account for the

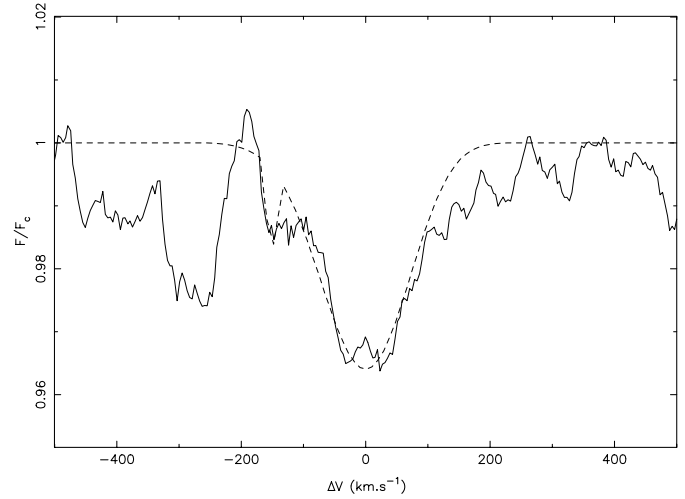


Fig. 10. Observed profile of He I 4471 Å (full line) and computed profile from a two component model, convolved by a rotation profile with $V_{rot}=80\text{ km s}^{-1}$ (dashed line). The observed profile was corrected for the star radial velocity, taken from Catala et al. (1999)

observational material at our disposal. As argued earlier, the CIR structure assumed to be responsible for the N V resonance lines, with temperatures of the order of 140,000 K, cannot produce the observed He I and He II line profiles. The regions responsible for the He I D3 blueshifted emission component must be cooler and located very close to the star's surface. In order to reconcile these requirements with those derived from the analysis of the N V resonance lines by Bouret et al. (1997), we may consider that the CIR exhibit a complex temperature structure, with several temperatures regimes: from 20,000 to 30,000 K to produce the He I D3 line as observed, around 140,000 K to account for the N V lines, and in the range 1–2 million K to explain the X-ray flux observed by ROSAT. Alternatively, we can imagine the presence of several families of CIR in the wind of AB Aur, with different densities and temperatures, depending on the strength of the shocks creating them.

In order to quantitatively assess the possibility that the He I D3 line is produced in such conditions and that the presence of CIRs in the wind does not affect the shape of neither the He I 4471 line nor the lines modelled up to now, we built a two-component model of the wind of AB Aur, proceeding as follows.

First, we introduced a hot geometrically thin region at the base of the wind model of BC99, between the minimum of temperature and the point where T_{max} (BC99) is reached. The density was set to the value required by He I D3, by artificially increasing the mass loss rate. The full set of radiative transfer equation and statistical equilibrium equations was solved for the corresponding model, yielding line source functions and opacities for all transitions in our He I-He II-He III atomic model. The emergent specific intensities were then calculated as described in Sect. 3.

In a second step, we removed the hot region from this model, re-calculated the emergent specific intensities, then evaluated

the contribution of the hot regions to the emergent specific intensity ($I^1(\nu, \theta)$) by subtracting the latter set of emergent specific intensities from the former.

The third step consists of the calculation of the emergent specific intensities from a BC99 model with its normal mass loss rate ($\dot{M} \approx 1.2 \times 10^{-8} M_{\odot} \text{ yr}^{-1}$), noted $I^0(\nu, \theta)$ in the following.

Finally, for calculations in the observer's frame, we simulated the presence of hot regions with high densities at the base of the wind when calculating the emergent flux as follows:

$$F(\nu) = \int_0^{2\pi} d\phi \int_{-\pi/2}^{\pi/2} \cos\theta [r(\theta, \phi)I^1(\nu, \theta) + [1 - r(\theta, \phi)] \times I^1(\nu_c, \theta)] d\theta + \int_0^{2\pi} d\phi \int_{-\pi/2}^{\pi/2} \cos\theta I^0(\nu, \theta) d\theta. \quad (1)$$

The weighting function $r(\theta, \phi)$ describes the distribution of the CIR in the wind. It is possible to simulate distributions of CIR more or less crowded near the equator. The same method was developed when calculating the contribution to the profile of C IV resonance line, of discrete high temperature regions in AB Aur's wind (Bouret et al. 1997).

Integration of the $r(\theta, \phi)$ function over all angles provides the filling factor f . The lower limit for the CIR density derived in Sect. 4.2.2 allows us to set an upper limit for the filling factor: $f \leq 0.18$. We also found that for $f \leq 2.5 \times 10^{-4}$, it is no more possible to obtain a significant emission on the blue side of the He I D3 line, whatever we choose for the density in the CIRs. It is possible to obtain a more constraining upper limit on f , thanks to the He I 4471 Å line. Observations (see Fig. 10) show that this line is centered on its rest wavelength, indicating that it is formed in a region where the velocity is low. This is consistent with the result from the BC99 model. In the framework of a two-components model, the presence of CIRs produces an additional absorption blue shifted by about 100 km s^{-1} . So as to achieve a reasonable agreement with the observed profile (i.e to prevent the He I 4471 Å line profile from being affected by the presence of CIRs) it is mandatory to assume that f is lower than 4.6×10^{-2} .

In summary, a two-component model as described here-above is consistent with observations for a filling factor in the range $2.5 \times 10^{-4} \leq f \leq 4.6 \times 10^{-2}$.

Figs. 10 and 11 show the profiles of He I 4471 Å and He I 5876 Å resulting from a two-component model built with BC99 + m7 of Table 1 (both with a low and a high value for the Doppler random velocity v_D in Fig. 11).

The agreement is qualitatively and quantitatively good in the case of He I 4471 Å, which supports our interpretation of the wind structure and give further credit to the constraints derived so far.

A closer look at the observed profile shows that an additional weak absorption component seems to develop blueward of the line center. We interpret this as possibly produced by the hot-dense component of the wind. We already mentioned (see Sect. 4.2.3) that this component gives rise to a blue-shifted absorption as long as $\rho \leq 6.1 \times 10^{-10} \text{ g.cm}^{-3}$. We computed

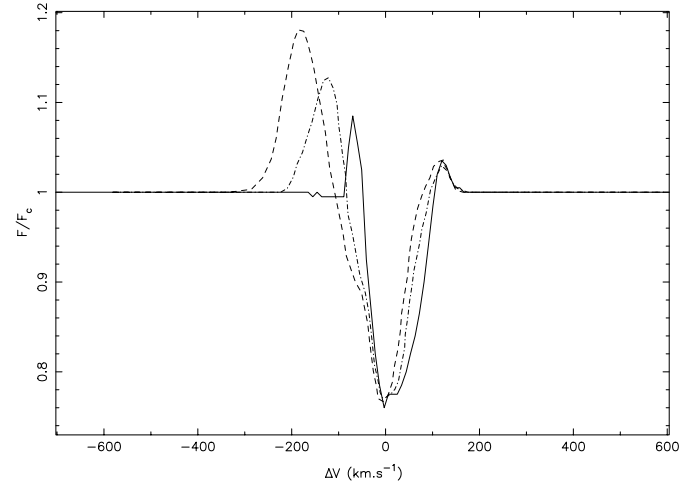


Fig. 11. Line profiles of He I 5876 Å resulting from simulation of wind with two components. The profile in full line is obtained with $v_D=10 \text{ km.s}^{-1}$, the profile in dashed-dotted line is obtained with $v_D=50 \text{ km.s}^{-1}$ and the profile in dashed line results from calculations with $v_D=75 \text{ km.s}^{-1}$.

the resulting profile from the same two-component model as for the He I D3 line and found that it has indeed the same kind of shape as the observed one, although not intense enough (see Fig. 10). On the other hand, Catala et al. (1999) found that the photospheric lines of AB Aur are asymmetric and generally composed of both a redshifted and a blueshifted component, the latter showing a periodic modulation in the velocity space ranging from -40 to -100 km s^{-1} . The 34 hrs period measured in 1996 is assumed to be the rotation period of the star itself. These observations led the authors to suggest that at least one expanding region, with velocities up to 150 km s^{-1} , exists deep enough inside the star, to contribute to the formation of photospheric lines. They also found that these regions have to be located at high latitudes. Therefore, if present, the contribution of CIRs to the He I 4471 Å line profile is very likely completely blended with this blue photospheric component. Finding a way to disentangle these two effects is beyond the scope of the present work.

As illustrated in Fig. 11, the profiles obtained with two components models are in qualitative agreement with the He I D3 profiles observed from time to time in AB Aur, with a blue-shifted emission component and an absorption component more or less centered at zero velocity (Böhm et al. 1996; Catala et al. 1999). In addition, the blueshifted emission component is formed in a high velocity part of the wind, so that its centroid velocity is sensitive to the velocity gradient near the base of the wind. If the wind is made of an alternation of fast and slow streams, the star's rotation can provide an explanation for the observed modulation of this component.

In the equatorial wind model, because the line formation region is very close to the photosphere, it is very likely that it is in corotation with the star, whose projected rotation velocity is $v \sin i = 80 \text{ km s}^{-1}$ (Böhm & Catala 1993). The line is therefore additionally broadened by rotation, which was already

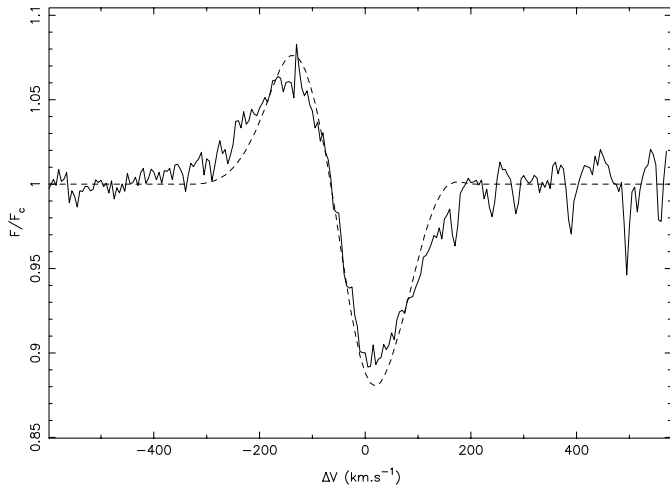


Fig. 12. Observed profile of He I 5876 Å and computed profile from a two component model with $f=7 \times 10^{-3}$ and $v_D=50 \text{ km.s}^{-1}$, convolved by a rotation profile (dashed line). The observed profile was corrected for the star radial velocity, taken from Catala et al. (1999)

mentioned in Böhm et al. (1996). This broadening induces in turn a weakening of the line intensity (so as to conserve the line equivalent width), which means that the filling factor must be increased to maintain an agreement with the observations. The He I D3 line in our model is formed in a compact region near the base of the wind, where in addition we can reasonably assume a solid rotation because of the presence of a magnetic field. Convolution of the computed profile with a rotation profile is therefore a reasonable approximation. The result is illustrated in Fig. 12 for the two component model with $f=7 \times 10^{-3}$ (analogous to the one found by Bouret et al. 1997).

Finally, we have checked thoroughly that the other lines studied previously, and well accounted for by the “standard” BC model (H α , Mg II and C IV resonance lines), are unchanged in our two-component model, i.e. they are not affected whatsoever neither by the slight change in velocity gradient near the base of the wind introduced in model BC99, nor by the addition of the CIR required by the He I D3 line. This is due to the fact that these other lines are formed either in the temperature maximum region of the chromosphere, or in the remote regions of the wind, so that they are not sensitive at all to the velocity gradient at the base of the wind, nor to the additional hot and dense regions that we have introduced to account for the blue emission component of the He I D3 lines. We also checked that our model does not produce any detectable He II λ 1640 Å line, does not affect the previously calculated N V resonance lines (Bouret et al. 1997), and does not produce any detectable emission nor absorption in the N IV λ 1718 Å line, which is also absent from the IUE spectra (Bouret et al. 1997).

4.4. The red emission: a three-component model

The red component of He I D3 behaving differently than the blue one, it is very likely that their regions of formation are distinct. This constitutes yet another evidence that the wind of

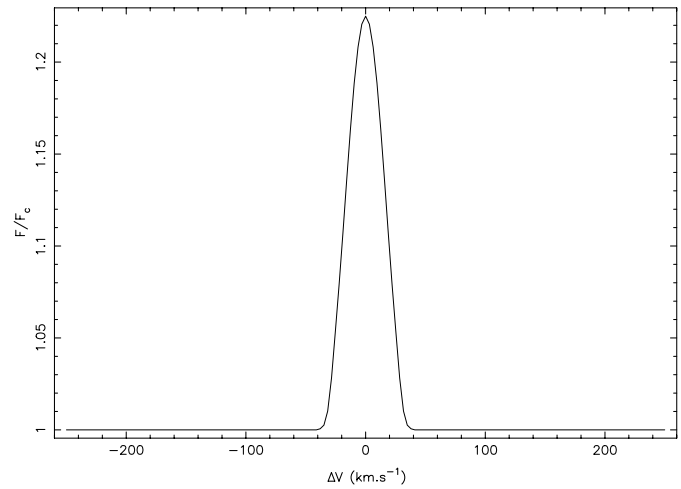


Fig. 13. Computed profile of He I 5876 Å for a hot, dense, region located around the pole of the star. The following parameter were adopted: $T_{hot}=30,000 \text{ K}$, $\dot{M}=10^{-7} M_{\odot} \text{ yr}^{-1}$, $r(\theta, \phi)=1$ if $\theta \leq 75^\circ$, $r(\theta, \phi)=0$ elsewhere

AB Aur is non homogeneous. This component appears episodically in emission, slightly redshifted, with no modulation of its centroid velocity (Catala et al. 1999). A tentative interpretation of this component given in Catala et al. (1999) assumes that it is produced by hot material accreting onto the stellar pole.

Although our model is not capable of dealing rigorously with accretion, we can nevertheless check quantitatively whether hot gas near the stellar pole can indeed produce an emission component with similar characteristics as observed. We mention that, in this context, the approach used by Muzerolle et al. (1998) constitutes another powerful and reliable tool to check this assumption on the process leading to the formation of the red component in emission.

We have simulated the presence of a hot and dense polar region by using Eq. 1, with a weighting function $r(\theta, \phi)$ strongly biased toward the pole, and setting $I^0 = 0$ so that only the contribution from the polar region is considered. The results of these calculations are presented in Fig. 13, and show that such a polar hot region can indeed produce a strong emission component. In our model, this emission component is centered at zero wavelength, as the velocity of the material producing it is near zero. We suggest that downward motions at the visible stellar pole will create the same kind of emission component, but redshifted, as observed, due to the plasma motion with respect to the observer. Such a redshifted emission component, whose maximum intensity is not decreased by rotation because it is formed at the pole, is likely to fill in the underlying absorption component produced by the two components model discussed in Sect. 4.3 (see Fig. 12).

On the other hand we note that the He I D3 line sometimes appears as depicted in dashed line in Fig. 1., i.e. with a blueshifted emission component, and a wide absorption component roughly centered at zero velocity (Catala et al. 1993; Böhm et al. 1996; Catala et al. 1999). Our calculated He I D3 line profile in the framework of the two-component model, i.e. without

a hot dense region at the stellar pole, is in agreement with such a profile. This indicates that, whatever the mechanism that forms the redshifted emission component when it is seen (e.g. polar accretion), this mechanism vanishes from time to time, leaving the He I D3 line with its basic blue-emission/central absorption profile. We suggest that this basic profile is formed in a wind structure similar to the one simulated in our two-component models, involving a roughly spherically symmetric wind and extended chromosphere with a mass loss rate of the order of $10^{-8} M_{\odot} \text{ yr}^{-1}$ and temperature near 17,000 K, and a set of hot and dense CIR occurring near the base of the wind.

We also suggest that the He I D3 line, when observed as a double emission line (see, e.g., the average profile of the MUSICOS 1996 campaign, depicted in solid line in Fig. 1), can be explained by a three-component model, involving (i) a more or less spherically symmetric wind with a mass loss rate and basic velocity and temperature structures similar to those of the BC99 model; (ii) a hot and clumpy medium produced e.g. by the expected CIR in the equatorial regions of the wind; (iii) a hot and dense region created by downflowing material at the poles, which produces the red emission component, hiding the underlying absorption component formed in the bulk of the chromosphere. This model is capable of explaining quantitatively all the observed characteristics of the He I-He II lines, including their temporal variability, as well as of all the other lines and continua observed in AB Aur.

5. Conclusion

Due to its high lying levels, the He I D3 line of AB Aur was considered to form in dense, hot regions, and is a perfect tool to probe these regions located at the base of the wind of this star.

Catala et al. (1999) discussed two possible interpretations of the characteristics of the He I D3 line. In the first one, the He I D3 lines, as well as other wind lines, are formed in an equatorial wind, a model first proposed by Pogodin (1992) to explain the episodic disappearance of the absorption components of the H α line PCygni profile. In this interpretation, the He I D3 line must be modulated by the star's rotation. The present paper was aimed at quantitatively checking the relevance of this interpretation.

A NLTE analysis of the formation of this line has provided new information on the physics in layers close to the star, from where it probably originates. Using the He I 5876 Å, as well as other He I and He II lines, we performed a systematic study of the influence of the physical parameters of our models, which provided a full set of constraints (temperature, density, gas velocity, location of the emitting layers) required to form these lines as observed. In particular, the question of the physical mechanism driving the He I 5876 Å line emission was addressed and we showed that departures from LTE are indeed implied.

In the framework of this interpretation of the He I D3 line, the presence of dense, hot regions, concentrated at low latitudes, at the base of AB Aur's wind, is necessary to explain the blue emission component which is always observed in this line. These dense hot regions can be naturally interpreted as due to co-rotating interaction regions near the base of the wind. In

these shocked regions, the material can be heated and its density can be enhanced, up to the values needed by the blue emission component of He I D3. This was simulated by a procedure similar to the one developed for studying the N V line in the wind of this star. These simulations again strengthen the interpretation of the rotational modulation of the He I D3 line as caused by the presence of streams of material rotating with the star.

The red component of the He I D3 line, when appearing in absorption, can be formed in the bulk of the *classical* chromosphere lying in the wind (Bouret & Catala 1998). When it appears in emission, this red component can be due to accretion onto the stellar pole, as our calculations suggest.

On the basis of the calculations presented in this paper, we conclude that this interpretation of the He I D3 line of AB Aur in terms of an equatorial wind + polar accretion is valid and consistent with all the available observational material.

The second possible interpretation of the He I D3 line proposed by Catala et al. (1999) involves both a disk-wind model, in which material is flowing out of an accretion disk, and polar accretion down to the stellar pole. In this case, the period of modulation of the He I D3 line is that of the disk rotation in the regions from where the wind originates. Although attractive, such a model also needs thorough quantitative checks, which is beyond the scope of this paper. In particular, this will require tools able to treat radiative transfer in highly non-homogeneous, non isotropic media, with important velocity fields, but outside the range of conditions under which the Sobolev approximation is applicable. Such tools are now under construction and could, in principle, be used for simulating either accretion columns, expanding and rotating winds, or disk-winds.

Acknowledgements. We thank Sylvie Sahal-Bréchet for providing us with her numerical code for calculations of collisional transition rates and John Tully for providing us with various atomic data. We also acknowledge fruitful discussions with Ivan Hubeny, about radiative transfer problems. Finally, we thank the MUSICOS collaboration for making data available to us. This work was performed while one of us (J.-C. B.) held a National Research Council-(NASA GSFC) Research Associateship.

References

- Appenzeller I., Jankovics I., Krauter J., 1983, A&AS 53, 293
- Appenzeller I., Jankovics I., Östreicher R., 1984, A&A 141, 108
- Babel J., Montmerle T., 1997, A&A 323, 121
- Basri G., Bertout C., 1989, ApJ 341, 340
- Beals C.S., 1950, Publ. DAO 9, 1
- Benson R.S., Kulander J.L., 1972, Solar Phys. 27, 305
- Berrilli F., Corciulo G., Ingrosso G., et al., 1992, ApJ 398, 254
- Berrington K.A., Kingston A.E., 1987, J. Phys. B 20, 6631
- Bertout C., Basri G., Bouvier J., 1988, ApJ 330, 350
- Beskrovnaya N.G., Pogodin M.A., Tarasov A.E., Sherbakov A.G., 1991, Pis'ma Astron. Zh. 17, 825 (Soviet Ast. Lett. 17, 349)
- Beskrovnaya N.G., Pogodin M.A., Nadjenov I.D., Romanyuk I.I., 1995, A&A 298, 585
- Böhm T., Catala C., 1993, A&AS 101, 629
- Böhm T., Catala C., 1994, A&A 290, 167
- Böhm T., Catala C., 1995, A&A 301, 155

- Böhm T., Catala C., Carter B., et al., 1996, *A&AS* 120, 431
Böhm T., Hirth G.A., 1997, *A&A* 324, 177
Bouret J.-C., Catala C., Simon T., 1997, *A&A* 328, 606
Bouret J.-C., Catala C., 1998, *A&A* 340, 163
Bouvier J., 1987, Ph.D. Thesis, Université Paris 7
Calvet N., Albarran J., 1984, *Rev. Mex. Astron. Astrofis.* 9, 35
Catala C., 1988, *A&A* 193, 222
Catala C., Kunasz P.B., Praderie F., 1984, *A&A* 134, 402
Catala C., Praderie F., Kunasz P.B., 1984, *A&A* 154, 103
Catala C., Praderie F., Felenbok P., 1986, *A&A* 182, 115
Catala C., Felenbok P., Czarny J., et al., 1986b, *ApJ* 308, 791
Catala C., Kunasz P.B., 1987, *A&A* 174, 158
Catala C., Böhm T., Donati J.-F., Semel M., 1993, *A&A* 278, 187
Catala C., MUSICOS collaboration, 1999, *A&A* 345, 884
Corcoran M., Ray T.P., 1997, *A&A* 321, 189
Corcoran M., Ray T.P., 1998, *A&A* 331, 147
Croswell K., Hartmann L., Avrett E.H., 1987, *ApJ* 312, 227
Donati J.F., Semel M., Cater B.D., et al., 1997, *MNRAS* 291, 658
Drew J.E., Proga D., Stone J.M., 1998, *MNRAS* L6-L10
Felenbok P., Praderie F., Talavera A., 1983, *A&A* 128, 74
Fernley J., Taylor K., Seaton M., 1987, *J. Phys. B* 20
Finkenzeller U., Mundt R., 1984, *A&AS* 55, 109
Grady C., Pérez M.R., Talavera A., et al., 1996, *A&AS* 120, 157
Grady C., Pérez M.R., Bjorkman K.S., et al., 1999, *ApJ* 511, 925
Gray D.F., 1992, In: *The observation and analysis of stellar photospheres*. 2nd edition
Grinin V.P., Rostopchina A.N., 1996, *Astron. Rep.* 40, 171
Hartmann L., Kenyon S.J., Calvet N., 1993, *ApJ* 407, 219
Hamman F., Persson S.E., 1992, *ApJS* 82, 285
Herbig G., 1960, *ApJS* 4, 337
Hillenbrand L., Strom S.E., Vrba F.J., Keene J., 1992, *ApJ* 397, 613
Hubeny I., 1988, *Comput. Phys. Comm.* 52, 103
Königl A., 1991, *ApJ* 370, L39
Kurucz R.L., 1979 *ApJS* 40, 1
Lignières F., Catala C., Mangeney A., 1996, *A&A* 314, 465
Mannings V., Sargent A., 1997, *ApJ* 490, 792
Marsh T.R., Kenneth A., Van Cleve J.E., et al., 1995, *ApJ* 451, 777
Mihalas D., 1978, In: *Stellar Atmospheres*. 2nd edition
Mihalas D., Stone M.E., 1968, *ApJ* 151, 293
Mihalas D., Kunasz P., 1978, *ApJ* 219, 635
Millan-Gabet R., Schloerb F.P., Traub W.A., et al., 1999, *ApJ* 513, L131
Mullan D.J., 1984, *ApJ* 283, 303
Muzerolle J., Calvet N., Hartmann L., 1998, *ApJ* 492, 743
Pezzuto S., Strafella F., Lorenzetti D., 1997, *ApJ* 485, 290
Pogodin M.A., 1992, *Pis'ma Astron. Zh.* 18, 1066
Praderie F., Simon T., 1986, *ApJ* 303, 311
Proga J., Stone J.M., Drew J.E., 1998, *MNRAS* 295, 595
Seaton M., 1962, *Proc. Phys. Soc.* 79, 1105
Shu F., Najita J., Ostriker E., et al., 1994, *ApJ* 429, 781
Skinner S., Brown A., Stewart R., 1993, *ApJS* 87, 217
Skrutskie M.F., Meyer M.R., Whalen D., Hamilton C., 1996, *AJ* 112, 2168
Sorelli C., Grinin V.P., Natta A., 1996, *A&A* 309, 155
Strafella F., Pezzuto S., Corciulo G.G., et al., 1998, *ApJ* 505, 299
Thé P.S., de Winter D., Pérez M., 1994, *A&AS* 104, 1
Tout C.A., Pringle J.E., 1995, *MNRAS* 272, 528
Vigneron C., Mangeney A., Catala C., Schatzman E., 1990, *Solar Phys.* 128, 287
Wiese W.L., Smith M.W., Glennon B.M., 1966, *NSRDS-NBS* 4, Vol. 1
Zinnecker H., Preibisch Th., 1994, *A&A* 292, 152